

Segregation kinetics and applications of brush-modified surfaces



**Thesis submitted in partial fulfillment for the award of
DOCTOR OF PHILOSOPHY
in
PHYSICS**

by
Samiksha Shrivastav

DEPARTMENT OF PHYSICS
**INDIAN INSTITUTE OF TECHNOLOGY
BANARAS HINDU UNIVERSITY
VARANASI - 221005**

ROLL NUMBER
19171001

YEAR OF SUBMISSION
06 August 2024

Dedicated to

My Family

and

My Grandfather

Lt. Dr. Radhey Shyam Yogi

Certificate

It is certified that the work contained in the thesis titled **Segregation kinetics and applications of brush-modified surfaces** by **Samiksha Shrivastav**, Roll Number **19171001**, has been carried out under my supervision and that this work has not been submitted elsewhere for a degree.

Signature: Awaneesh Singh Supervisor Co-Supervisor External Supervisor
(Affiliation) (Affiliation) (Affiliation)

Assistant Professor
Department of Physics
Indian Institute of Technology
(Banaras Hindu University)
Varanasi-221005

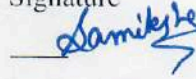
Declaration

I, **Samiksha Shrivastav**, certify that the work embodied in this thesis is my own bona-fide work and carried out by me under the supervision of **Dr. Awaneesh Singh** from 29 July 2019 to 6 August 2024 at the **Department of Physics**, Indian Institute of Technology (BHU), Varanasi. The matter embodied in this thesis has not been submitted for the award of any other degree/diploma. I declare that I have faithfully acknowledged and given credits to the research workers whenever and wherever their works have been cited in my work in this thesis. I further declare that I have not wilfully copied any others' work, paragraphs, text, data, results, etc., reported in journals, books, magazines, reports dissertations, theses, etc., or available at websites and have not included them in this thesis and have not cited as my own work.

Date **06/08/2024**


Signature

Place **Varanasi**



Certificate by the Supervisor

It is certified that the above statement made by the student is correct to the best of my knowledge.

Signature:  Supervisor
Assistant Professor (Affiliation)
Department of Physics
Indian Institute of Technology
(Banaras Hindu University)
Varanasi-221005

Co-Supervisor
(Affiliation)

External Supervisor
(Affiliation)

Signature of the Head of the Department

(Department)
HEAD/विभागाध्यक्ष

भौतिकी विभाग/Deptt. of Physics
ना०प्री०सं०/(का०हि०वि०)/IIT (BHU)
वाराणसी/Varanasi-221005

Copyright Transfer Certificate

Title of the Thesis : **Segregation kinetics and applications of brush-modified surfaces**

Name of the Student : **Samiksha Shrivastav**

Copyright Transfer

The undersigned hereby assigns to the Indian Institute of Technology (Banaras Hindu University) Varanasi all rights under copyright that may exist in and for the above thesis submitted for the award of the **Doctor of Philosophy (Ph.D)** in **Physics**.

Date *06/08/2024*

Signature *Samiksha*

Place *Varanasi*

Samiksha Shrivastav

Note: However, the author may reproduce or authorize others to reproduce material extracted verbatim from the thesis or derivative of the thesis for author's personal use provided that the source and the Institute's copyright notice are indicated.

Acknowledgements

I want to take this opportunity to express my deep appreciation to all those who have been instrumental in my PhD journey. First and foremost, I am truly grateful to my respected supervisor, Dr. Awaneesh Singh, from the Department of Physics at IIT (BHU), Varanasi. His guidance, motivation, patience, and unwavering support have been invaluable throughout my doctoral experience. It has been an honor to have him as my mentor. The knowledge and skills I have acquired under his supervision will undoubtedly benefit me for many years to come.

I am also profoundly grateful to my RPEC members, Dr. Shradha Mishra from the Department of Physics at IIT (BHU), Varanasi, and Dr. Lavanya Selvaganesh from the Department of Mathematics at IIT (BHU), for their valuable insights and feedback during my presentations. Additionally, I appreciate the collaboration with Prof. Sampa Saha from the Department of Material Science and Engineering at IIT Delhi on my Ph.D. projects. Special thanks to my collaborators, Ms. Ifra, Ms. Shubhashree S. Pradhan, and Ashank from the Department of Material Science and Engineering at IIT Delhi.

I am deeply thankful to my fellow lab mates (Avinash, Ashish, Devendra, Vanshika, Ankita and, Ayushi) and past lab members (Anish and Sachin) from the Multiscale Simulation Lab (MSS) group in the Department of Physics for their unwavering assistance and support. I am truly grateful for Avinash's unwavering dedication and expertise in overcoming research challenges. Ashish and Devendra consistently provide invaluable perspectives and enthusiasm, enhancing our academic and non-academic conversations. Their contributions enrich our collective understanding and stimulate insightful exchanges.

My gratitude extends to my institute, IIT (BHU), for providing essential resources, computing facilities, and access to the PARAM SHIVAY supercomputing facility throughout my research. I want to acknowledge the department's academic and administrative staff for their continuous support. I am grateful for the Junior Research Fellowship and Senior Research Fel-

lowship awarded to me by IIT (BHU). I want to express my sincere gratitude to the Science and Engineering Research Board (SERB) for the Early Career Research Award (ECRA) Fellowship Grant (ECR/2017/002529). Additionally, I am thankful for the travel grant (ITS/2023/002521) that enabled me to attend the 28th International Conference on Statistical Physics, Statphys28, Japan.

I want to express a special note of appreciation to my grandmother, my parents, my uncle, and my aunt for their unwavering support and strength. I also thank my siblings and cousins - Shidhant, Vedant, Anekant, Saksham, Sakshi, Srajan, Aprajita, Devansh, and Suyash - for their constant love and care. My gratitude also extends to my friends, Priya, Kartika, Nidhi, Monia, Shweta, Vindya, Sachin, Shubham, Anuvrat, Shivam, Harsh, Santosh, batch mates, seniors, and everyone who has been part of this journey. Kartika feels like a home away from home for me. She has supported me a lot. I have learned many things from my first roommate and friend, Vani di. Having a senior roommate is a rewarding experience that offers valuable learning opportunities and support.

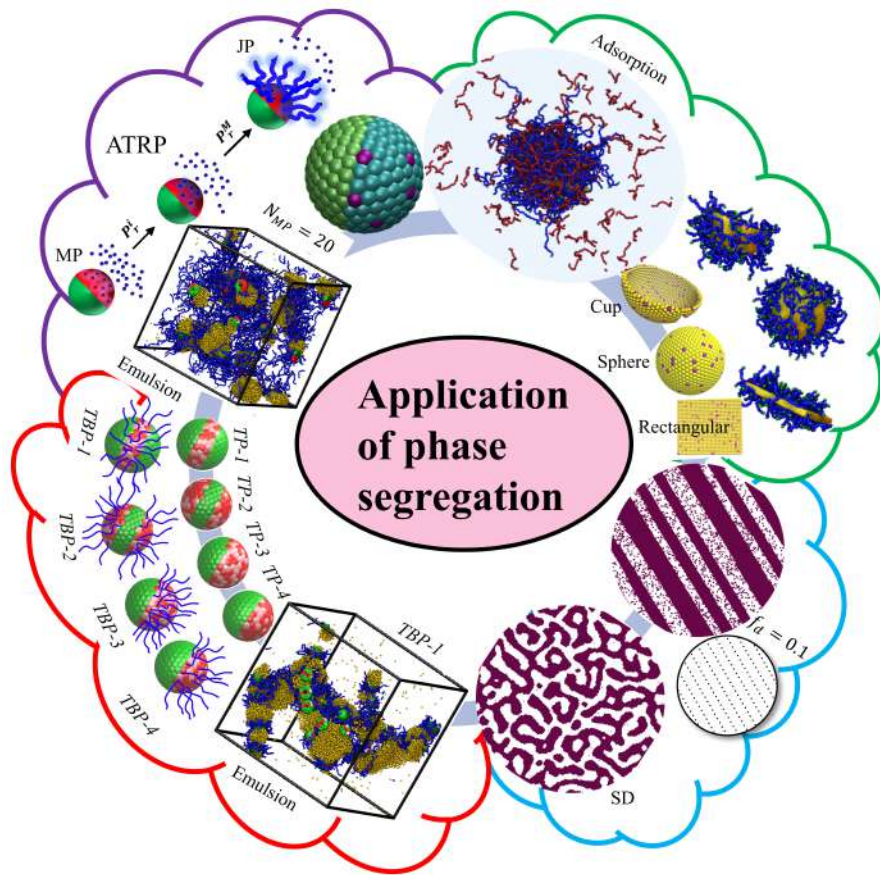
In particular, I want to express my deep appreciation to Richa Singh. She has been an incredible source of support over the past year, providing encouragement during moments of doubt and assisting in improving my overall well-being. Having Richa as a roommate has been a blessing, and I am profoundly grateful for her presence and support.

I want to thank Ashish wholeheartedly for the incredible support you have given me throughout my PhD journey. Your friendship means the world to me, and I am incredibly grateful to have had you by my side through it all.

Lastly, I also want to express my deepest gratitude to Pawan for your unwavering support over the past two years in my PhD journey. Your understanding, encouragement, love, and patience have been invaluable during these challenging times. Thank you for being there for me. Many thanks to Poonam for providing me with delicious food. Her tasty meals have been greatly appreciated.

Above all, I offer my heartfelt thanks to Mahadev and Kamakhya Ma for their divine blessings throughout my research work.

Abstract



My thesis explores various aspects of phase separation kinetics under external influences. Specifically, we studied the effect of polymer brush-modified macroparticle surfaces on biopolymer adsorption using dissipative particle dynamics (DPD) simulations. Our research analyzed the formation of oil-in-water emulsions and their stability with brush-modified Janus particles (JPs). We synthesized these polymer brushes using the atom transfer radical polymerization (ATRP) method. Additionally, in a separate work, we analyzed the impact of impurities on phase separation in $2d$ Ising model systems through Monte Carlo simulations.

Chapter 1 provides a comprehensive overview, delving into phase separation kinetics, domain growth, coarse-graining, quantifying various physical observables, and the simulation techniques utilized in the upcoming chapters.

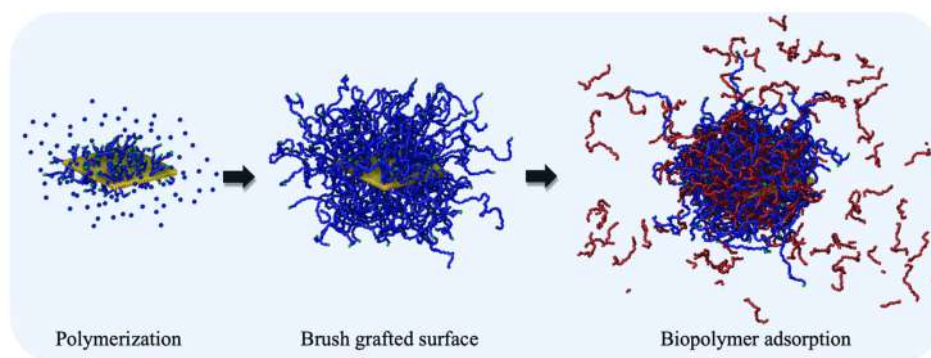


Fig. 1: Biopolymer adsorption on the brush-modified surface [1].

In Chapter 2, we examined the modification of microparticle (MPs) surfaces embedded with initiators through ATRP brush growth. This process led to the MPs acquiring a more spherical shape. We studied three types of surfaces: cup-shaped, spherical, and flat (rectangular/disc-shaped) and modified them with polymer brushes. Initially, we established the chemical kinetics of brush growth, including monomer conversion and reaction rates. Subsequently, we analyzed the structural changes during the brush modification by computing the spatial density distribution, radial distribution function, radius of gyration, hydrodynamic radius, and shape factor. We studied enzyme adsorption on ATRP-brush-modified particles, focusing on the effects of initiator concentration, polymer brush length, and biopolymer chain length, which can be used for enzyme immobilization. Our results showed that biopolymer adsorption increased with longer brush length, higher initiator concentration, and enhanced biopolymer concentration. The flat surfaces accommodated more biopolymers at saturation compared to cup-shaped or spherical surfaces. We validated these results experimentally. The table of contents of this work is shown in Fig. 1.

In Chapter 3, we numerically explore the stabilization of Pickering emulsions by brush-modified JPs using DPD simulations validated through experimental data. Each JP has a

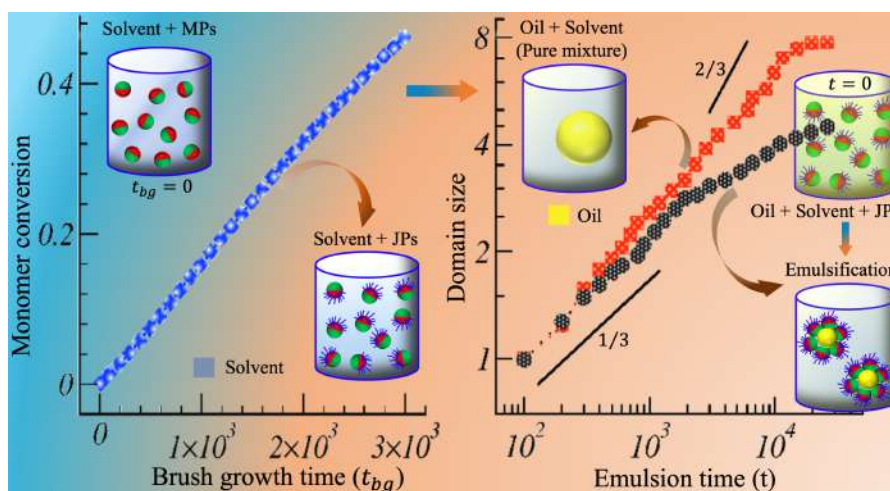


Fig. 2: Oil in water emulsion via brush-modified Janus Particle [2].

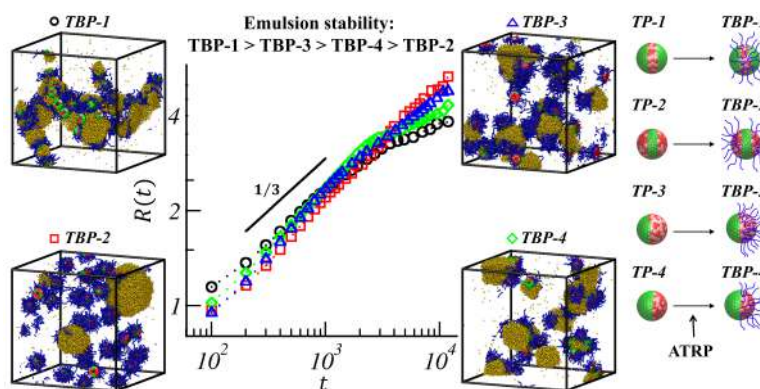


Fig. 3: Oil in water emulsification via tri-compartmental brush-modified Janus particle [3].

hydrophobic half (without brushes) and a hydrophilic half (brush-modified surface) with polymer brushes grown using ATRP. Initially, we analyzed the chemical kinetics of brush growth. We found that the number of JPs, grafted brush density, and brush length significantly influence the stability of oil-in-water emulsions. Furthermore, we examined the evolution kinetics and stability of emulsions by analyzing the growth of average domain size and scaling functions. This study elucidates the relationship between JP characteristics and Pickering emulsion stability. The table of contents for Chapter 3 is shown in Fig. 2.

In Chapter 4, an extension of Chapter 3, we investigate the formation of oil-in-water emulsions using brush-modified tricompartmental particles (TPs/JPs). Our objective was to

understand how the functionality of TPs influences the stability of Pickering emulsions by varying the brush length, grafting density, and types of JPs (TP-1 to TP-4) based on the polymer brush growth region on the microparticle surface. We examined stability and morphological changes using the radial distribution function, length scale growth, and scaling functions. The table of contents for Chapter 4 is shown in Fig. 3. Chapter 5 presents the segregation kinetics

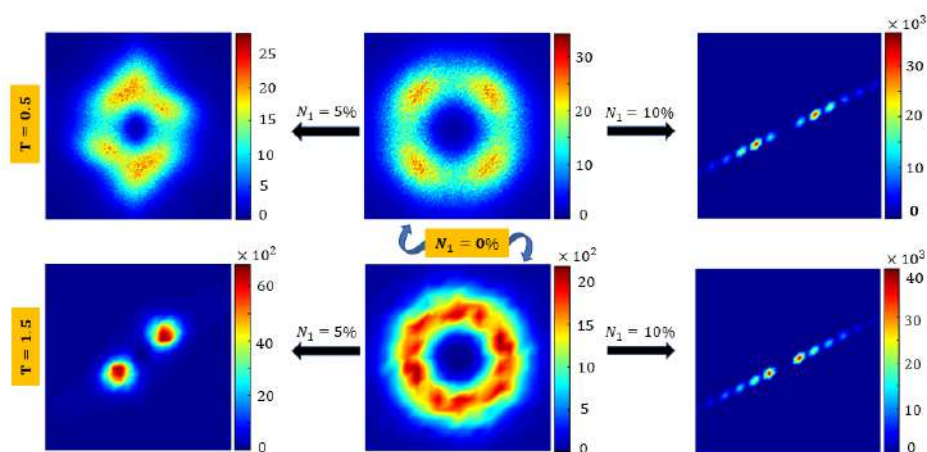


Fig. 4: Segregation kinetics under the influence of bond disorder [4].

of a $2d$ Ising system with varying bond disorders. We found that different quench temperatures affect the growth kinetics and scaling properties of the system. As the disorder increases, the morphologies transition from isotropic bicontinuous patterns to anisotropic strips and lamellae. At lower disorder levels, there is transient growth at deep quenches, while higher disorder levels lead to the formation of lamellar patterns. High disorder significantly alters scaling behavior, causing the length scale to freeze at finite sizes. In Fig. 4, we show the table of contents for Chapter 5.

Finally, in Chapter 6, we provide a comprehensive summary and conclusion of the research and findings presented in the thesis.

Table of contents

List of figures	xvi
List of tables	xxx
Nomenclature	xxx
1 Introduction	1
1.1 Phase separation kinetics	1
1.2 Domain growth and coarsening	2
1.3 Coarse-graining	9
1.4 DPD simulation	10
1.4.1 Modeling parameters	15
1.4.2 Modeling of polymer chain	16
1.5 Formation of microparticles	17
1.6 Radical polymerization	18
1.6.1 Atom transfer radical polymerization (ATRP) process	19
1.7 Brush modification of microparticles via ATRP	21
1.7.1 Application of brush-modified surfaces	23
1.8 Monte Carlo simulation/ Ising model	25
1.8.1 Gluaber spin-flip dynamics	29
1.8.2 Kawasaki spin-exchange dynamics	29

1.9	Physical observable	30
1.9.1	The correlation function and the structure factor	32
1.9.2	Growth laws and Characteristics length scale	33
1.9.3	Radial distribution function	36
1.9.4	Shape and size characterization of polymer	37
1.10	Overview of the thesis	39
2	Biopolymer adsorption on differently shaped brush-modified surfaces	42
2.1	Introduction	42
2.2	Methodology and model parameter	45
2.2.1	Preparation of microparticles	45
2.2.2	Surface fabrication of microparticles via ATRP	47
2.2.3	Modeling the biopolymer adsorption	47
2.3	Result and discussion	49
2.3.1	Simulation study	49
2.4	Conclusion	64
3	Stabilizing Pickering emulsion by brush-modified Janus Particles	67
3.1	Introduction	67
3.2	Simulation methodology	70
3.2.1	DPD simulation	70
3.2.2	Morphology characterization function and the characteristic length scale	71
3.2.3	Constituting microparticle	72
3.2.4	Brush modification of microparticles	73
3.3	Result and discussion	76
3.4	Conclusion	89

4	Emulsion formation via polymer brush-modified tri-compartmental microparticles	92
4.1	Introduction	92
4.2	Simulation methodology	95
4.2.1	DPD simulation	95
4.2.2	Constituting microparticle	96
4.2.3	Brush-modification of microparticles	98
4.2.4	Characterization function for morphology and the characteristic length scale	98
4.3	Results and discussion	99
4.4	Conclusion	110
5	Phase separation kinetics of binary mixture in the influence of bond disorder	112
5.1	Introduction	112
5.2	Simulation model and implementation	115
5.2.1	Basic step with disordered site	115
5.2.2	Correlation function and structure factor	118
5.2.3	Scaling functions and length scale	119
5.3	Simulation results and discussion	120
5.3.1	Pure binary mixture: $f_d = 0.0$	120
5.3.2	Binary mixtures with the lower fractions of bond disorder: $f_d = 0.02, 0.05$	122
5.3.3	Binary mixture with a higher fraction of bond disorder: $f_d = 0.1$. . .	128
5.4	Summary and conclusion	134
6	Summary and future plan	137
6.1	Summary	137
6.2	Future plan	138
	References	141

List of figures

1	Biopolymer adsorption on the brush-modified surface [1].	x
2	Oil in water emulsion via brush-modified Janus Particle [2].	xi
3	Oil in water emulsification via tri-compartmental brush-modified Janus particle [3].	xi
4	Segregation kinetics under the influence of bond disorder [4].	xii
1.1	The phase diagram of a typical ferromagnetic system is shown. The system exhibits significant changes at a specific point, denoted as T_c and $h_c = 0$, known as the second-order critical point. Below T_c , a first-order transition line appears at $h = 0$, indicating a boundary in the phase diagram where the system stabilizes in one of two equilibrium phases characterized by either up or down spin orientations.	3
1.2	The snapshots show the evolution of a spin-1/2 ferromagnet using a MC simulation of the Ising model on a $2d$ lattice with periodic boundary conditions. Time is measured in units of Monte Carlo steps (MCS), and the temperature is kept at $T = 1.0$. In the visualizations, maroon regions represent up spins, and white regions represent down spins.	4

1.3	The phase diagram of a binary (AB) mixture is governed by the volume fraction of component A ($\phi_A = 1 - \phi_B = \phi$) and the temperature (T). A second-order critical point occurs at $\phi = 0.5$, $T/T_c = 1.0$. Above the solid coexistence curve, the mixture remains in a homogeneous state. Below this curve, the system undergoes phase separation, forming distinct A-rich and B-rich regions. The dashed lines represent the spinodal curve, marking zones of instability [5,6]. Between the coexistence and spinodal curves, the system is metastable, becoming unstable once it crosses below the spinodal lines [5,6].	7
1.4	The phase ordering dynamics in a binary mixture (AB) occur when the system is quenched to a temperature (T) below the critical temperature ($T_c \simeq 2.269$). In this case, the temperature is set at $T = 1.0$. The system size is ($L_x \times L_y = 512 \times 512$). The snapshots are from MC simulations of the Ising model using spin-exchange Kawasaki kinetics at different MCS. In the visualizations, maroon and white regions represent A-rich and B-rich domains, respectively.	8
1.5	A schematic representation of coarse-graining for polyethylene ($-CH_2 - CH_2-$) _n	10
1.6	(a) The schematic representation of the cut-off radius, r_c . (b) Conservative pair potential $U(r_{ij})$ as a function of the distance r_{ij} between beads i and j	12
1.7	Bead spring model	16
1.8	Cup, spherical and rectangular microparticles.	18
1.9	A few examples of polymer topologies that were obtained from the CRP method.	19
1.10	Shows the monomer conversion in (a) and the reaction rate kinetics $\ln[M_0/M_u]$ in (b) with time.	20
1.11	Schematic representation of reaction steps of ATRP process	22

1.12 (a) This image displays a cup microparticle with a fraction of initiators (pink beads) on its concave and convex surfaces. This cup-MP has inner and outer radii of $7.7r_c$ and $8.0r_c$, respectively. Figs. (b), (c), and (d) depict the polymerized microparticles with varying initiator concentrations of $c_i = 1\%$, 2.5% , and 5.0% . The polymerization time extends up to $t_{BG} = 1500\tau$. Additionally, the blue beads symbolize the PBs.	23
1.13 (a) Shows the application of polymer brush-modified anisotropic particles. (b) shows the cylindrical pores exhibited high drug loading capacity [7].	24
1.14 Phase ordering dynamics in an off-critical binary mixture. The quenched temperature is ($T = 1.0$). The system size is (512^2). These snapshots are derived from MC simulations of the Ising model employing spin-exchange Kawasaki kinetics. In the visualizations, maroon and white regions represent A -rich and B -rich regions, respectively.	31
1.15 The two-point equal-time spatial correlation function in (a) and its corresponding structure factor in (b) for the critical binary fluid mixture evolved at time $t = 60$ in $d = 3$	34
1.16 Characteristics length scale of phase separating binary (AB) mixture over time on a log-log scale.	34
1.17 Shows the unscaled correlation function in (a) and the corresponding scaling function in (b) at different times.	35
1.18 (a-b) Illustrates the scaling of the structure factor at different times. The solid line represents the Porod's tail with a slope of $-(d + 1)$ where $d = 2$	35
1.19 Radial distribution function of a phase separating simple binary fluid system at a time $t = 60$	37

- 2.1 (a) The graph shows the monomer conversion ($Conv_M$) over time (t_{BG}) for three different initiator concentrations: $c_i = 1.0\%$, 2.5% , and 5.0% . (b) The plot illustrates the change in the monomer conversion rate, $\log([M]_0/[M]_{ut})$ over time. (c-e) display ATRP brush-modified cup surfaces at different c_i up to $t_{BG} = 1500$. (f-h) show the corresponding cross-section plots at $l_z = 25$, indicating brush density variation around CS. The color bar is at the extreme right. 50
- 2.2 The figure shows the comparison of the temporal variation of monomer conversion $Conv_M$ in (a) and the natural logarithm of the ratio of initial monomer concentration to monomer concentration at time t , $\log([M]_0/[M]_{ut})$, in (b) at the surfaces of the cup (CS) in black, spherical surface (SS) in red, and rectangular surface (RS) in green curves for a $c_i = 5.0\%$ initiator concentration embedded on their surfaces. 51
- 2.3 Radius of gyration R_g (a), the hydrodynamic radius R_h (b), and the shape factor $\rho_{sf} = R_g/R_h$ (c) are shown with the ATRP brush growth time t_{BG} for CS. The curves in black, red, and green represent for the initiator concentrations of $c_i = 1.0\%$, 2.5% , and 5.0% , respectively, embedded on the CS surface. 52
- 2.4 The radial distribution function with radial distance, $g(r)$ vs. r is shown in (a) and (b) the density distribution, ρ_z , depicts the distribution of the grown ATRP-brushes along the z-direction at time $t_{BG} = 1500$ at CS for various initiator concentrations: $c_i = 1.0\%$ (black symbols), 2.5% (red symbols), and 5.0% (green symbols), corresponding to the snapshots shown in Fig. 2.1(c-e). 54
- 2.5 Comparison of the temporal variations of $Conv_M$ (a) and $\log([M]_0/[M]_{ut})$ (b) at the cup surface (CS, black curve), spherical surface (SS, red curve), and rectangular surface (RS, green curve) for $c_i = 5.0\%$ 55

- 2.6 The ATRP brush-modification of CS, SS, and RS for $c_i = 5.0\%$ up to the brush growth (polymerization) time $t_{BG} = 400$ (a–c), 800 (d–f), and 1500 (g–i). (j–l) The brush density variation in the xy cross-section at $l_z = 25$ corresponds to the snapshots in (g–i). 57
- 2.7 Comparison of the (a) radius of gyration R_g , (b) hydrodynamic radius R_h , and (c) shape factor ρ_{sf} vs. the polymerization time t_{BG} for the brush-modified CS (black curve), SS (red curve), and RS (green curve), respectively, at $c_i = 5\%$. 57
- 2.8 Comparison of the radial distribution function (RDF) $g(r)$ of ATRP brushes around (a) CS, (b) SS, and (c) RS at different brush lengths observed at various polymerization times for $c_i = 5\%$ 58
- 2.9 The estimated fraction of adsorbed biopolymers, ϕ_{bA} , is shown for brush-modified CS (black symbols), SS (red symbols), and RS (green symbols) with different biopolymer fractions: (a) $\phi_b = 2 \times 10^{-2}$, (b) $\phi_b = 4 \times 10^{-2}$, and (c) $\phi_b = 8 \times 10^{-2}$ in the solution with $c_i = 5\%$. The adsorption process is monitored for $t_{bA} = 3000$ 59
- 2.10 Comparison of the biopolymers adsorption for different brush lengths grown up to $t_{BG} = 400$, 800, and 1500 on CS, SS, and RS, respectively. The corresponding brush lengths are shown in the legend. The adsorption is for each brush length until $t_{bA} = 3000$. (a–c) display $g(r)$ vs. r for the biopolymers around CS, SS, and RS beads, respectively. (d–f) show the temporal variation in the adsorbed fraction of biopolymers, ϕ_{bA} 62
- 2.11 Assessment of the adsorption of biopolymers with different chain lengths: $l_b = 1$ (black curve), $l_b = 10$ (red curve), and $l_b = 25$ (green curve) on brush-modified surfaces: CS, SS, and RS. The adsorption process continued for $t_{bA} = 3000$. (a–c) show the RDF plot $g(r)$ vs. r , while (d–f) display the temporal variation of the adsorbed fraction of biopolymers, ϕ_{bA} 63

- 3.1 (a) The diagram highlights the initiation and propagation reactions and key phases in ATRP reactions for brush growth. (b) Pink and blue glowing beads represent the active initiator and monomer, while the reacting initiator and monomer are shown by pink and blue beads connected by a solid blue line. Unreacted monomers are depicted by the typical blue beads. (c) The hydrophobic surfaces S_1 and S_2 are depicted by green and red beads, and the yellow bead represents oil. For clarity, water beads are not shown in this or any forthcoming figures in this work. (d) The homogeneous structure $t = 0$ of water, oil, and JPs is illustrated. 76
- 3.2 (a) Monomer conversion ($Conv_M$) is shown for different initiator concentrations: $c_i = 1.0\%$ (in black), 2.5% (in red), and 5.0% (in green) of MP over brush growth time (t_{bg}). Within the system, there are 20 MPs. ATRP is done for $t_{bg} = 1.2 \times 10^3$. The rate kinetics are displayed in the inset as $\ln([M]_0/[M]_u)$ vs. t_{bg} . (b) Monomer conversion is displayed for various $t_{bg} = 1.2 \times 10^3$ (in black), 1.8×10^3 (in red), and 3.0×10^3 (in green) at a constant $c_i = 5.0\%$. The corresponding reaction rate kinetics are displayed in the inset. The polymer brush growth (in blue) on the S_2 surfaces (in red) over time is shown in the right panel. For better visibility, a zoomed image of a brush-modified JP is shown to enhance the clarity. 78

- 3.3 Oil emulsion evolution through brush-modified JPs at different time t values: 5.0×10^2 , 2.0×10^3 , 8.0×10^3 , and 2.6×10^4 are shown (a-d). The blue beads represent the polymer brushes. There is also a close-up picture of a JP molecule modified by a brush for better understanding. To ensure picture clarity, the water droplets are not shown. The volume fraction of oil is $\phi_0 = 5 \times 10^{-2}$. (e) The scaled $C(r,t)$ vs. $r/R(t)$ plots at $t = 2.0 \times 10^3$, 8.0×10^3 , 1.6×10^4 , and 2.6×10^4 are denoted by black, red, green, and blue symbols. The solid line guides the zero-crossing of $C(r,t)$. The inset shows the corresponding unscaled $C(r,t)$ vs. $r/R(t)$ plots. (f) Characteristics length scale, $R(t)$ vs. t for the evolution snapshots in panels (a–d) is shown in black symbols. The red curve exhibits the same for the pure oil and water mixture. Their corresponding late-time morphologies are shown in the inset. The solid lines with slope $1/3$ and $2/3$, representing growth exponents, are drawn for reference. 80
- 3.4 (a) A comparison of $C(r,t)$ vs. $r/R(t)$ for different values of c_i (1.0% in black, 2.5% in red, and 5.0% in green) is shown for $t = 2.6 \times 10^4$. (b) The corresponding length scale, $R(t)$ vs. t is plotted on a log-log scale during the emulsification time. The insets show the corresponding morphologies of oil emulsion in the solvent by brush-modified JPs for a fixed $Conv_M \approx 19.45\%N_M$. 82

- 3.5 (a) The graph shows the radial distribution function, $g(r)$ vs. r , for oil around the S_1 surface. A close-up view of a brush-modified JP molecule is depicted for improved clarity. (b) Comparison of a scaling function, $C(r,t)$ vs. $r/R(t)$, for three different brush densities represented by different symbols at $t = 2.6 \times 10^4$. (c) The graph illustrates the time variation of length scale, $R(t)$, for three different brush densities. The inset of Figure (a), (b), and (c) respectively, shows the corresponding oil emulsion morphologies by brush-modified JPs with the same brush length $l_b \approx 18$ but different brush densities, $\rho_b \approx 2.89 \times 10^{-2}$, 7.26×10^{-2} , and 14.5×10^{-2} 84
- 3.6 The graph in (a) shows the radial distribution function, $g(r)$ vs. r , for oil around the S_1 surface with different symbols indicating various brush lengths. In (b), there is a comparison of scaling functions ($C(r,t)$ vs. r and $R(t)$) at $t = 2.6 \times 10^4$. (c) presents the characteristic length scale ($R(t)$ vs. t) on a logarithmic scale. Additionally, the inset of Figures (a) and (b) shows the corresponding evolution morphologies of oil emulsion by brush-modified JPs for brush lengths $l_b \approx 0, 24$ and $l_b \approx 37, 60$, respectively. 86
- 3.7 The graph displays the length scales, $R(t)$ vs. t , for the oil emulsion at different numbers (and sizes) of JPs. Specifically, N_{MP} is equal to 20 (black curve), 40 (red curve), and 80 (green curve) for a fixed brush length, l_b , which is approximately 66. The inset shows the corresponding evolutionary morphologies of oil-in-water emulsion at $t = 2.6 \times 10^4$ 89
- 4.1 Figure shows the TP-1, TP-2, TP-3, and TP-4 type MPs. 97

- 4.2 (a) The graph shows the monomer conversion ($Conv_M$ vs. t_{bg}) during the growth of polymer brushes with different initiator concentrations. For TP-1 and TP-4 MPs, the initiator concentration (c_i) is about 3% of (n_{MP}), while for TP-2 and TP-3 MPs, the initiator concentration is about 6% of n_{MP} . The curves on the graph represent the monomer conversion for four types of MPs: TP-1 (black), TP-2 (red), TP-3 (green), and TP-4 (blue). The initiators are embedded on the outer surface of the MPs, and the study involves a total of 30 MPs. . . . 100
- 4.3 Comparison of the temporal variation of monomer conversion ($Conv_M$) in (a) and $\ln([M]_0/[M]_u)$ in (b) for TP-1 (black), TP-2 (red), TP-3 (green), and TP-4 (blue) MPs. In (a), the monomer conversion demonstrates a linear behavior at early times and converges towards one at later times for all cases. In (b), there is a linear relationship between natural logarithm of ($[M]_0/[M]_u$) and time. The green and red curves show a slight deviation from linearity when $Conv_M \rightarrow 1.0$ at much later times. 101
- 4.4 The images (a-d) illustrate the oil-in-water emulsion morphology using polymer brush-modified four types of MPs: TP-1, TP-2, TP-3, and TP-4. The length of the polymer brush is constant at $l_b \simeq 7$, and the emulsification time is set at $t = 1.2 \times 10^4$. Solvent (water) beads are omitted for clarity. In (e-g), the radial distribution function (RDF) $g(r)$ vs. r , the scaled correlation function $C(r,t)$ vs. $r/R(t)$, and the characteristic length scale $R(t)$ vs. t are presented at the emulsification time, $t = 1.2 \times 10^4$ for brush modified TP-1, TP-2, TP-3, and TP-4. The oil concentration in the system is set at $\phi_0 = 5.0 \times 10^{-2}$ 102
- 4.5 Comparison in the length scales ($R(t)$ vs. t) for the oil-in-water emulsion morphology of (a) TP-1 and TP-4 type MPs and (b) TP-2 and TP-3 type MPs at $l_b \simeq 7$ and $l_b \simeq 14$, respectively. The emulsification time is set at $t = 1.2 \times 10^4$ and $\phi_0 = 5.0 \times 10^{-2}$ 105

- 4.6 (a) Comparison of RDF ($g(r)$ vs. r) for the emulsification time $t = 1.2 \times 10^4$ for oil beads around S_1 surface at a constant brush density, where overall monomer conversion in the system is kept constant for all TPs. (b) Shows the characteristic length scale ($R(t)$ vs. t) on a log-log scale for TP-1, TP-2, TP-3, and TP-4 MPs denoted by black, red, green, and blue symbols, respectively. 106
- 4.7 The graphs (a-c) illustrate the evolution of oil emulsion morphology using polymer brush-modified TP-1 MPs at different brush densities (ρ_b) of approximately 0.01, 0.02, and 0.05, while maintaining a constant brush length (l_b) of approximately 7 for an emulsification time of $t = 1.2 \times 10^4$. Graph (d) compares the radial distribution function (RDF) ($g(r)$ vs. r) for oil beads around the S_1 surface. (e) shows the time variation of length scale ($R(t)$ vs. t) at different brush densities for TP-1 MPs. 107
- 4.8 (a-c) Morphologies of oil emulsion for different brush densities, $\rho_b \simeq 0.02$, 0.05, and 0.11 for TP-3 at $t = 1.2 \times 10^4$. (d-f) Morphologies for TP-4 with $\rho_b \simeq 0.01$, 0.02, and 0.05 at $t = 1.2 \times 10^4$. The brush length, $l_b \simeq 7$, was kept constant for all the cases. Comparison of the time variation of length scale ($R(t)$ vs. t) is displayed at different brush densities for TP-3 in (g) and TP-4 in (h) for the emulsification time up to $t = 1.2 \times 10^4$ 109
- 4.9 Comparison of the length scales ($R(t)$ vs. t) for the oil-in-water emulsion for TP-1 to TP-4 MPs for (a) lower, (b) moderate, and (c) high brush density at $l_b \sim 7$. For TP-1 and TP-4, the brush density varies as $\rho_b \simeq 0.01$, 0.02, and 0.05, and for TP-2 and TP-3, the brush density varies as $\rho_b \simeq 0.02$, 0.05, and 0.11. 110

- 5.1 The $2d$ Ising model on a square lattice is depicted in the following images. In (a), black circles represent pure sites, while red circles represent disordered sites with up (blue triangles) and down (green triangles) spins randomly assigned. (b) and (c) illustrate the standard Kawasaki spin-exchange kinetics probability and the exchange interaction (J_{ij}) between neighboring spins: (b) when two nearest-neighbor (nn) spins are at pure sites, and (c) when at least one nn spin is at a disordered site. Moreover, (d-f) show sections of disordered sites on a $2d$ square lattice of size $N = L^2$, where $L = 512$, for disorder fractions (f_d) of 0.02, 0.05, and 0.1, respectively. This figure provides a comprehensive visual representation of the Ising model with disordered sites. 116
- 5.2 Evolution snapshots for a critical binary (AB) mixture at time $t = 4 \times 10^6$ MCS for temperatures (a) $T = 0.5$, (b) $T = 1.0$, and (c) $T = 1.5$, where the parameter $f_d = 0.0$ represents the pure case. The spatial intensity fluctuation of $S(k_x, k_y)$ is shown in the insets in (a-c). The datasets at $T = 0.5, 1.0$, and 1.5 for the scaling plot of $C(r, t)$ vs. $r/l(t)$ align neatly on a single curve. The plotting of $S(k, t)l(t)^{-2}$ vs. $kl(t)$ is displayed in the inset. The structure factor follows Porod's law, $S(k, t) \sim k^{-3}$ for $k \rightarrow \infty$, and is followed by the structural factor tail. The log-log plot of the characteristic length scale, $l(t)$ vs. t , is displayed in (e) for the evolution seen in (a-c). The solid black line represents the expected growth exponent for the pure case, which is $\phi_{eff} = 1/3$. The variation of ϕ_{eff} as a function of $1/l(t)$ is shown in the inset figures. 121

- 5.3 (a-c) Evolution snapshots are shown at $t = 4 \times 10^6$ MCS for $T = 0.5, 1.0,$ and $1.5,$ respectively, for $f_d = 0.02.$ Different symbols are used to represent the scaling plots of $C(r,t)$ vs. $r/l(t)$ in (d) and $S(k,t)l(t)^{-2}$ vs. $kl(t)$ in (e) for $f_d = 0.02$ at three quench temperatures. The log-log plot of the length scale $l(t)$ vs. t for all three cases is displayed in (f). The effective growth exponent, ϕ_{eff} vs. $1/l(t)$ is depicted in (g) for $T = 1.0$ and $T = 1.5,$ with the inset of (g) showing it for $T = 0.5.$ 123
- 5.4 (a-c) Evolution snapshots are shown at $t = 4 \times 10^6$ MCS for $T = 0.5, 1.0,$ and $1.5,$ respectively, for $f_d = 0.05.$ Different symbols are used to represent the scaling plots of $C(r,t)$ vs. $r/l(t)$ in (d) and $S(k,t)l(t)^{-2}$ vs. $kl(t)$ in (e) for $f_d = 0.05$ at three quench temperatures. The log-log plot of the length scale $l(t)$ vs. t for all three cases is displayed in (f). The effective growth exponent, ϕ_{eff} vs. $1/l(t)$ is depicted in (g) for $T = 1.0$ and $T = 1.5,$ with the inset of (g) showing it for $T = 0.5.$ 125
- 5.5 Plots of $S(k_x, k_y)$ at $t = 4 \times 10^6$ MCS for the following cases: (a) $f_d = 0.02,$ and (b) $f_d = 0.05,$ at $T = 1.5.$ The spatial intensity variation associated with the structure factor, $S(k_x, k_y),$ is displayed in (c–d), revealing the system’s orientation and anisotropy. 127
- 5.6 Plot $S(k_x, k_y)$ vs. k_x along the lattice diagonals for $f_d = 0.02$ at $T = 0.5$ (black and red curves) and $T = 1.0$ (green and blue curves) at $t = 4 \times 10^6$ MCS. For $f_d = 0.05,$ (b) shows the same data as in (a). The changes in the spatial scattering intensity at $T = 1.0$ for $f_d = 0.02$ and 0.05 are displayed in the insets (a) and (b). 128

- 5.7 We compare the structure factors without spherical averaging, $S(k_x, k_y)$ vs. k_x along the lattice diagonals at $T = 1.5$ and $T = 1.0$ for $f_d = 0.02$ and $f_d = 0.05$, respectively. The nonoverlapping of curves confirms the presence of structural anisotropy in the system. 129
- 5.8 (a-c) Evolution snapshots at $f_d = 0.1$ in the asymptotic limit for $T = 0.5, 1.0$, and 1.5 , respectively. (d) Plotting $C(r, t)$ vs. $r/l(t)$ for the evolutions in (a-c) at $T = 0.5$ (black symbol), $T = 1.0$ (red symbol), and $T = 1.5$ (green symbol). (e) Plotting $S(k, t)l(t)^{-2}$ vs. $kl(t)$ for the data sets in (d). (f) A length scale log-log plot with $l(t)$ vs. t . (g) A comparison of $S(k_x, k_y)$ for morphologies at $T = 1.5$ and $T = 0.5$ along the lattice diagonals. 130
- 5.9 Phase separation for three different system sizes, $N = L^2$ where $L = 128, 256, \text{ and } 512$, respectively, for a given fraction of disorder, $f_d = 0.1$ at a quenching temperature $T = 1.0$. The top row displays the arrangement of disorder sites, and their top-left corners show the zoomed version of a section of the disorder sites. The bottom row demonstrates the corresponding statistically similar phase-separated morphologies (long stripes or lamellar patterns), oriented in different directions (along with the higher number of disorder sites) 131
- 5.10 Phase separation for the different fractions of disorder at a fixed system size ($N = L^2; L = 512$), quenched at $T = 1.5$. In the top row, we show the distribution of disorder sites $f_d = 0.05$ and 0.1 . The bottom row demonstrates corresponding stripe patterns of different types and orientations (along with the higher number of disorder sites) 132

-
- 5.11 (a) Plot of $C(r,t)$ vs. $r/l(t)$ for different levels of disorder, where $T = 0.5$ for $t = 4 \times 10^6$ MCS and $f_d = 0.0$ (black curve), 0.02 (red curve), 0.05 (green curve), and 0.1 (blue curve). (b) For the datasets in (a), a plot of $S(k,t)l(t)^{-2}$ vs. $kl(t)$ is shown. The variation in scattering intensity over space at $T = 0.5$ is depicted for $f_d = 0.02$ in (c), $f_d = 0.05$ in (d), and $f_d = 0.1$ in (e). 133
- 6.1 Schematic of our simulation study on the self-assembly of nanorods in polymer matrices or binary fluid mixtures. We will utilize DPD and MD simulation techniques. In this work, we first report on the self-assembly and phase behavior of photo-sensitive nanorods in multicomponent fluids to evaluate the role of entropic and enthalpic factors that control the aggregation/dispersion process of nanorods. Second, we study the self-assembly of electrically charged photo-sensitive nanorods in phase-separating fluids. Next, we assess the effect of nanorods on the evolution morphology, growth law, and scaling phenomena in such systems. 139

List of tables

2.1	The interaction parameter a_{ij} used in the simulation for different DPD beads.	49
3.1	The interaction parameter a_{ij} used in the simulation for different DPD beads.	70
3.2	Details of the number of beads constituting the MPs of various sizes.	73
4.1	The interaction parameter a_{ij} used in the simulation for different DPD beads.	98